PAPER

High performance magnetorheological elastomers strengthened by perpendicularly interacted flax fiber and carbonyl iron chains

IOP Publishing Smart Materials and Structures
Smart Mater. Struct. 29 (2020) 025010 (13pp) https://doi.org/10.1088/1361-665X/ab5e49

High performance magnetorheological elastomers strengthened by perpendicularly interacted flax fiber and carbonyl iron chains

Quan Shu, Li Ding, Xinglong Gong[1], Tao Hu and Shouhu Xuan[1]

CAS Key Laboratory of Mechanical Behavior and Design of Materials, Department of Modern Mechanics, CAS Center for Excellence in Complex System Mechanics, University of Science and Technology of China, Hefei, Anhui 230027, People's Republic of China

E-mail: xuansh@ustc.edu.cn and gongxl@ustc.edu.cn

Received 22 August 2019, revised 14 October 2019
Accepted for publication 3 December 2019
Published 6 January 2020

Abstract

This work reported a novel high performance flax fiber (FF) strengthened magnetorheological elastomer (FF-MRE), whose mechanical property was improved by the unique three-dimension (3D) topologic strengthening structure composed of flax fiber and perpendicular carbonyl iron particles (CIPs) chains. Both the tensile and shear properties of this polydimethylsiloxane (PDMS) based FF-MRE were obviously influenced by the content of CIPs and flax fiber layers. In comparison to the anisotropic pure MRE, the tensile strength of FF-MRE with two layers of flax fiber increased as high as 87%. Importantly, when the content of the CIPs was kept at 70 wt%, the magnetorheological (MR) effect reached 184%. It was found that the CIPs chains were vertical to the flax fiber and the crosslink 3D topologic structure strengthened the PDMS matrix. Under the external magnetic field, the relative MR effect increased with increasing of the magnetic dipole-dipole interaction. Due to the enhanced stretch-ability, a flexible and magneto-controllable gripper was developed based on the flax fiber strengthened MRE, which demonstrated a delicate activity on actuation. This material is expected to have broad potential in active control and intelligent actuator.

Supplementary material for this article is available online

Keywords: magnetorheological elastomer, flax fiber, topologic structure, carbonyl iron, chains

(Some figures may appear in colour only in the online journal)

1. Introduction

Magnetorheological elastomers (MREs), whose mechanical properties can be quickly and reversibly changed by applying a magnetic field, have attracted increasing interests for their broad applications in vibration absorber [1–6], dampers [7–9], sensors [10, 11], actuators [12–16], and robots [17, 18]. Traditionally, the isotropic MREs consist of ferromagnetic particles randomly distributed in the polymer matrix, while the anisotropic MREs are prepared by dispersing magnetic particles into polymer matrix and the magnetic particles form chain-like or columnar structures to increase the magnetorheological (MR) effect [19, 20]. The MR effect refers to the ratio of the magnetic induced modulus to the initial storage modulus ($\Delta G/G_0$). Under the external magnetic field, the magnetic particles interact with each other via the magnetic dipole-dipole action and thus the polymer matrix is strengthened. Therefore, the MR effect and mechanical properties of the MRE can be controlled by varying the assembling structures of magnetic particles and their further interaction with polymer [21–23].

During the past decade, various efforts have been conducted to improve the mechanical property of MRE by modulating the polymer matrix, such as natural rubber [24–26], silicon rubber [27, 28], the resin [29, 30], PU (polyurethane) sponge [31], gels [32–34] and PDMS

[1] Authors to whom any correspondence should be addressed.

(polydimethylsiloxane) [35]. It was found that the polyurethane/silicone rubber hybrid MRE showed better MR effect than that of MRE based on pure Si-rubber or PU matrix [36]. Similarly, the curing process was also controlled to enhance the MR effect and the tensile strength [37]. Moreover, when the crosslink ratio decreased, the zero-field modulus (G_0), magnetic-induced modulus (ΔG) and the influence of Payne effect of the MRE had an increasing trend [38]. As we know, the mechanical properties of the anisotropic MRE in the direction vertical to the columnar structures are stronger than those of the direction parallel to the columnar structures. However, the tensile strength of the MRE in the parallel direction is very important for their practical applications. Unfortunately, most of the previous researches were focused on vertical MR performance, but the investigation on the parallel direction has not been well taken.

The three-dimensional (3D) scaffolds such as the sponge and foam have been introduced into the smart materials to improve the mechanical performance [39–42]. It is found that the interconnected skeleton can not only maintain the elasticity but also strengthen tensile stress of PU sponge reinforced MR material. The carbonyl iron particles (CIPs) were doped into the PDMS matrix to form the porous sponge and final MR-sponge exhibited high stretch-ability due to the flexible 3D bone structure [43]. Flax fiber is one of weaved natural fibers which can be added as a strengthening additive to composites because of the light weight and high stiffness. The epoxy matrix composite reinforced with woven flax fiber textiles showed a high fracture toughness and the PDMS-flax fiber possessed wonderful shear, compressive and tensile properties [44, 45]. As mentioned in the above analysis, the CIPs can form chain-like structures in the MRE. Therefore, the 3D scaffold consists of perpendicularly interacted flax fiber and CIPs chains will be favorable in improving the mechanical properties of MREs. In addition, the vertically located flax fiber is also helpful for strengthening the parallel directional mechanical behavior.

In this work, a novel high performance MRE with high mechanical performance is designed by introducing the unique 3D topologic structure composed of perpendicularly interacted flax fiber and CIPs chains into the PDMS matrix. The influence of factors (such as layers of flax fiber, content of CIPs, pre-structure and vulcanization ratio) on the mechanical properties are systematically studied. Both the shear properties and tensile properties of the as-prepared have been investigated. The proposed mechanism demonstrates that the perpendicularly interacted flax fiber and the vertical cross-link 3D topologic structure strengthen the PDMS matrix. Due to the enhanced stretch-ability and magnetic field dependent mechanical behavior, a flexible and magneto-controllable gripper integrated with inner electromagnets is developed. The advantages of real-time controllable, convenient operation and flexible movement endow the 3D topologic MRE with wide application prospects in active control and intelligent robots.

2. Experimental section

2.1. Materials

Polydimethylsiloxane (PDMS) produced by Dow Corning Corporation (USA) was used as the matrix, and Sylgard 184 was used as the vulcanizing agent. The carbonyl iron particles (CIPs, type CN) with average particle diameter of 3.85 μm produced by BASF (Germany) were used as ferromagnetic particles and dispersed in the matrix. Flax fibers (Jiujiang Yarnfan Textile Co. Ltd, China) contained 4 strands of fibers per centimeter were used.

2.2. Experiments

First, 2 g vulcanization agent was added into 40 g PDMS (20:1). Then, different CIPs with mass fractions (30 wt%, 40 wt%, 50 wt%, 60 wt%, 70 wt%) were introduced into the above precursor. When investigated the effect of the vulcanization ratios, the CIPs mass fraction was controlled at 50 wt%, and the MR precursors with different vulcanization ratios (10:1, 20:1, 30:1) were prepared using the similar process. All the above materials were stirred with glass rod for 10 min until they were blended homogeneously. After that, the PDMS/CIPs mixture was dried in the vacuum oven to eliminate bubbles for 15 min. Then, the mixture was poured into the mold and spread homogeneously to the position of 1 mm at the bottom of the mold. The flax fiber was spread into the position of 2 mm at the mold along the longitudinal direction. Afterwards, the mixture was further poured into the position of 3 mm at the mold to entirely cover the flax fiber. Next, the other layer of flax fiber was laid on the mixture matrix in the position of 4 mm, and then poured the mixture precursor into the position of 5 mm at the mold. At this time, the sample contained 2 layers of flax fiber was prepared. The preparation method of flax fiber with different layers contained in the matrix was similar to the above method. After extracting the bubbles for 15 min in vacuum, the specimen was ultimately located under the magnetic field generator. It was pressed tightly and cured under 100 °C, under applying a 1 T magnetic field with 15 min. Here, the controllable samples with different CIPs mass fractions, flax fiber layers, cured ratios were prepared using the similar process.

In this work, the flax fiber strengthened MRE was defined as FF-MRE under applying the magnetic field. The FF-MRE without applying the magnetic field during the preparation process was defined as FF-MRE-unpre. The FF-MREs with different mass fractions of CIPs were defined as FF-MRE-X, where X was the mass fraction. The FF-MREs with different layers of flax fiber were defined as YFF-MRE, where Y was the number of flax fiber layers.

2.3. Characterization

The microstructure of the MRE samples were observed by environment scanning electron microscope (SEM, Philips of

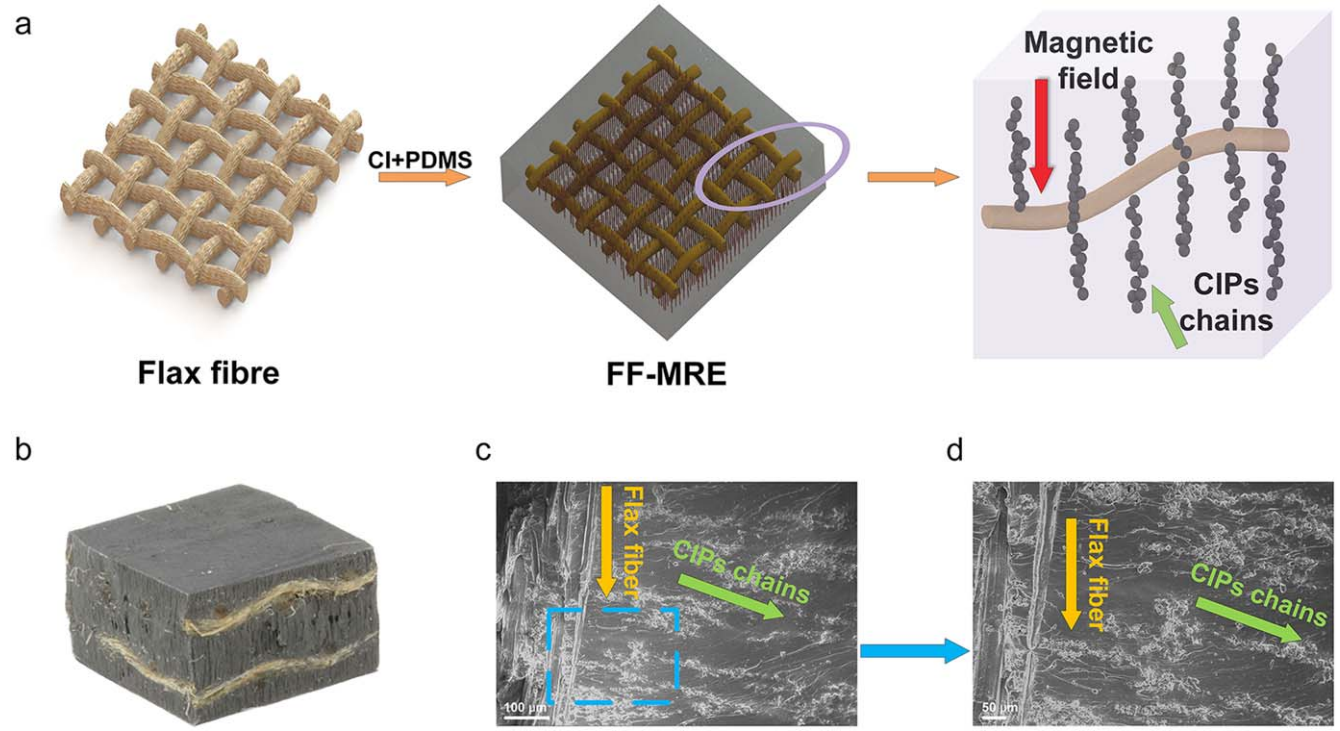

Figure 1. Preparation process of (a) FF-MRE; (b) The optical image of 2FF-MRE; (c), (d) SEM images of 2FF-MRE.

Holland, model XL30 ESEM-TMP) under 20 kV. The hysteresis loop of the MRE was tested by Hysteresis Measurement of Soft and Hard Magnetic Materials (HyMDC Metis, Leuven, Belgium).

2.3.1. The test of rheological properties. The dynamic mechanical properties of MRE samples were tested with a modified dynamic mechanical analyzer (DMA, Triton Technology Ltd, UK, mode Tritec 2000B). During the test, a self-made electromagnet was applied with a variable magnetic field from 0 to 800 mT. The magnetic field and the shear stress were parallel and perpendicular with the direction of the particle chains, respectively. The shear amplitude was 0.1% and the frequency was from 10 to 40 Hz. In this experiment, the dimension of MRE samples for dynamic mechanical tests was 10 mm × 10 mm × 5 mm. Each shear test was repeated at least 3 times and each result was basically consistent, which could ensure the repeatability and accuracy of the test results.

2.3.2. The test of tensile performance. An electronic universal testing machine (MTS criterion 43, MTS System Co., America) was applied for tensile fracture tests. The force and displacement data were recorded to analyze the mechanical properties of the MRE. The strain rate was 0.6 mm s^{-1}, and the tensile length was set at 60 mm. In this quasi-static tensile test, the dimension of MRE samples was 20 mm × 4 mm × 5 mm for the central tensile area (ISO 37: 2005).

3. Results and discussions

3.1. Preparation and characterization of FF-MRE

Figure 1(a) illustrates the schematic diagram of FF-MRE prepared by doping flax fiber into the PDMS based MREs. During the preparation, the CIPs were uniformly mixed within the PDMS precursor. After being spread on the flax fiber, the PDMS was cured under applying an external magnetic field. Therefore, the CIPs reassembled to form chain-like structures along the direction of magnetic field and they were vertical to the flax fiber plane. Figure 1(b) shows the picture of the 2FF-MRE, which indicates the two layers of flax fiber are well confined within the MREs. As shown in the SEM images of the FF-MRE (figure 1(c)), the flax fiber bonds well with the PDMS matrix and no obvious crackle is observed in the interface. The high magnification SEM image (figure 1(d)) indicates that the CIPs are assembled to form the chain-like microstructures along the applied magnetic field. More importantly, these CIPs chains are vertical to the flax fiber, which agrees well with our hypothesis. Therefore, the CIPs chains perpendicularly interact with the flax fiber to form the 3D topologic structure within the PDMS matrix. Originated from the soft magnetic CIPs, the FF-MRE is also magnetizable. The FF-MRE with different CIPs mass fractions can be saturated at a small magnetic field strength of

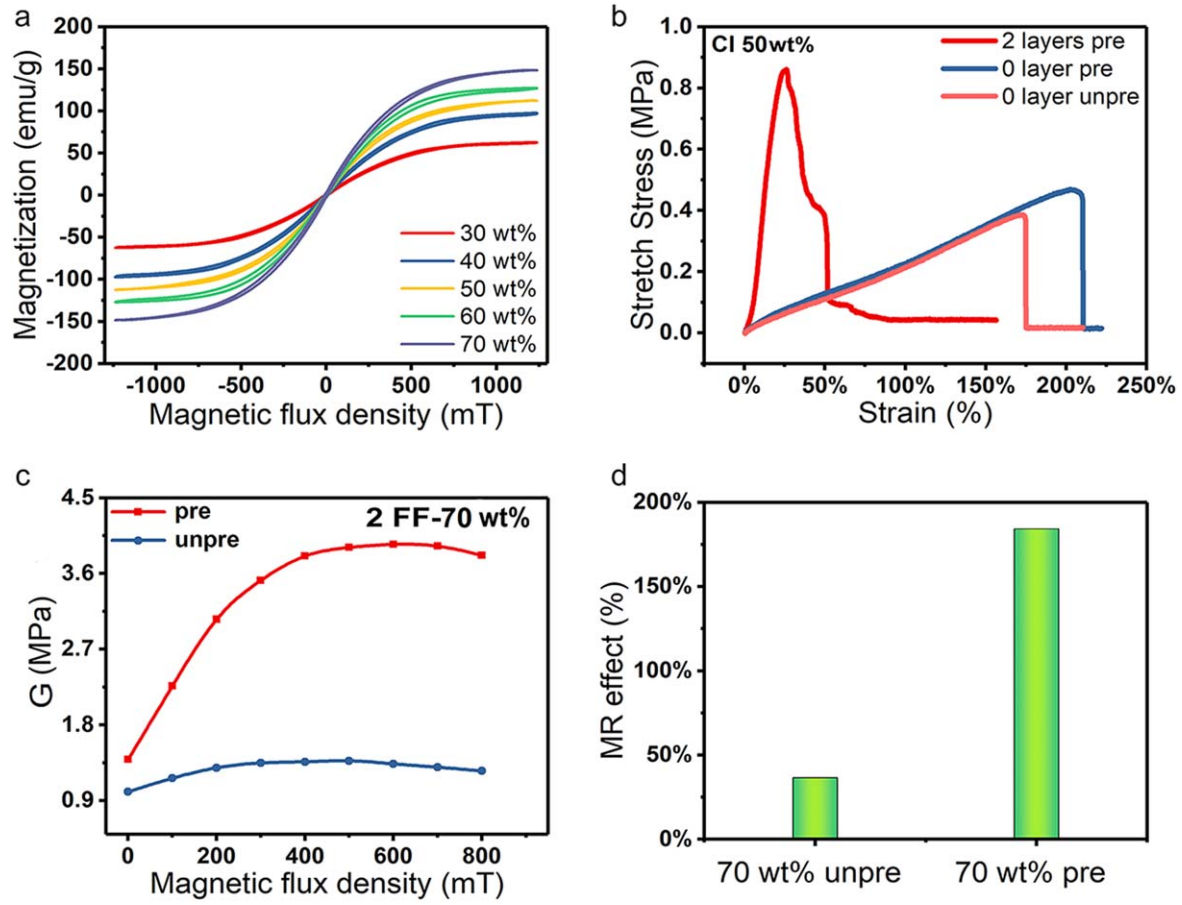

Figure 2. (a) Magnetization of FF-MRE-unpre with different CIPs mass fractions; (b) Tensile properties of 2FF-MRE-50 wt% and MRE-50 wt%; Rheology properties of 2FF-MRE and 2FF-MRE-unpre: (c) shear storage modulus and (d) MR effect of 70 wt% pre and 70 wt% unpre.

400 mT. The saturation magnetizations (M_s) of FF-MRE-unpre with different CIPs mass fractions are 62.7 emu g^{-1} (FF-MRE-unpre-30 wt%), 97.6 emu g^{-1} (FF-MRE-unpre-40 wt%), 112.3 emu g^{-1} (FF-MRE-unpre-50 wt%), 127.2 emu g^{-1} (FF-MRE-unpre-60 wt%) and 148.5 emu g^{-1} (FF-MRE-unpre-70 wt%), respectively (figure 2(a)).

Figure 2(b) shows the tensile stress-strain curves of 2FF-MRE and pure MRE. The maximum tensile stress of 2FF-MRE is 0.9 MPa which the corresponding fracture strain is 26%, while the maximum tensile stress value of isotropic pure MRE is 0.4 MPa and anisotropic pure MRE is 0.5 MPa. Obviously, the tensile strength of the 2FF-MRE is higher than the pure MRE, which also indicates the mechanical performance for the MRE is critically improved. Interestingly, different from the stress drops to 0 MPa after tensile fracture for pure MRE, the stress for the 2FF-MRE is reduced slowly. The camera video indicates the PDMS based MRE matrix is broken firstly during the tensile process (movie S1, S2 is available online at stacks.iop.org/SMS/29/025010/mmedia). Then, with further increasing the tensile strain, the stress slowly decreased to 0 MPa with the flax fiber fractured. This analysis demonstrates the adhesion between the flax fiber and matrix is high, and flax fiber effectively improves the tensile strength of FF-MRE. As a result, it can be concluded that the parallel directional mechanical behavior of MRE has been successfully strengthened by flax fiber.

Because of the the CIPs' random dispersion in the FF-MRE-unpre and the soft magnetic nature, the FF-MREs presented typical rheological properties. Keeping the CIPs mass fraction at 70 wt%, the shear storage moduli (G) of both the 2FF-MRE-unpre and 2FF-MRE increase with the magnetic field (figure 2(c)). Meanwhile, the MR effect of the 2FF-MRE is also investigated. The relative MR effect of 2FF-MRE is as high as 184% which is much higher than the 2FF-MRE-unpre (36%, figure 2(d)). Since the chain-like CIPs aggregations are in favor of increasing the magnetic dipole-dipole interactions, the 2FF-MRE prepared by the pre-structure process exhibits a higher MR effect. Based on the above analysis, it is found that FF-MREs show both high tensile strength and wonderful magnetorheological performance due to its unique 3D topological structure composed of perpendicularly interacted flax fiber and CIPs chains.

3.2. Effect of CIPs mass fraction on the FF-MRE

Figure 3(a) is the SEM image of the 2FF-MRE-30 wt%, which demonstrates the CIPs form chain-like structures and they perpendicularly interact with flax fiber. When the CIPs mass fractions further increase to 50 wt% and 70 wt% (figures 3(b), (c)), the CIPs chains distributed much more densely in the matrix. Figure 3(d) illustrates the stress-strain curves of 2FF-MREs with different CIPs mass fractions.

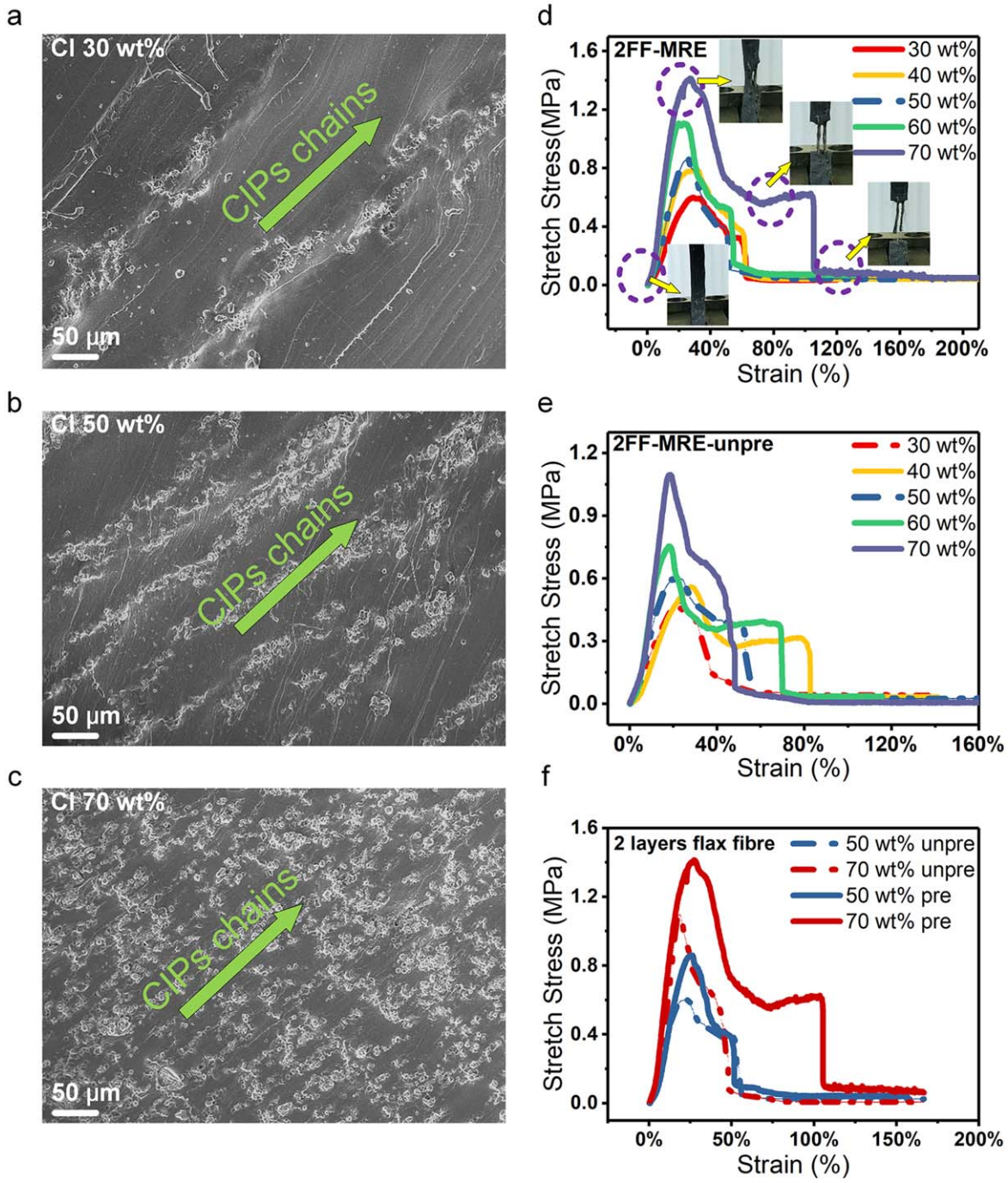

Figure 3. SEM images of 2FF-MREs with different CIPs mass fractions: (a) 30 wt%, (b) 50 wt% and (c) 70 wt%; Tensile fracture images of (d) 2FF-MRE, (e) 2FF-MRE-unpre and (f) comparison of tensile fracture process with 50 wt% and 70 wt% CIPs mass fraction.

When the CIPs mass fractions vary from 30 wt% to 70 wt%, the maximum tensile fracture stress of 2FF-MREs gradually increases from 0.6 MPa to 1.4 MPa. During the tensile process, the crack propagation occurs firstly in the PDMS matrix of 2FF-MREs. When the stress reaches a critical value, the matrix is fractured completely during the stretching process. At this time, the 2FF-MRE matrix is completely broken and reaches the maximum tensile fracture stress but the flax fiber is still not broken. Therefore, with further increasing of the strain, the stress keeps a relatively stable stage. This stage represents the stretching process of fibers in the PDMS matrix. As soon as the fibers are stretched to the critical value, they are fractured. In this case, the stress value suddenly drops to 0 MPa.

Here, the tensile behaviors of FF-MRE-unpre, in which the CIPs are randomly dispersed, are also investigated. Similarly, a two fracture process is clearly observed in all the samples (figure 3(e)). With increasing of the CIPs mass fractions, the tensile fracture stress gradually increases, due to the increasing of the CIPs chains. The slope of the stress-strain curve before tensile fracture represents the Young's modulus. Typically, the Young's modulus of FF-MRE-unpre

increases with the CIPs mass fraction. Figure 3(f) illustrates the comparison of tensile stress-strain curves of 2FF-MRE and 2FF-MRE-unpre by keeping the CIPs mass fraction at 50 wt% and 70 wt%, respectively. The maximum tensile stress value of 2FF-MRE-50 wt% and 2FF-MRE-70 wt% is 0.9 MPa and 1.4 MPa, respectively, while the corresponding value of 2FF-MRE-unpre are 0.6 MPa (50 wt%) and 1.1 MPa (70 wt%). It is obvious that the CIPs exhibit the classic particle-strengthening effect, and the pre-structure process can significantly improve the tensile properties of FF-MREs.

The maximum shear storage modulus of 2FF-MRE-unpre increases from 0.2 MPa (30 wt%) to 1.4 MPa (70 wt%) (figure 4(a)). As shown in figure 4(b), the maximum shear storage modulus of 2FF-MRE significantly increases from 0.3 MPa (30 wt%) to 3.9 MPa (70 wt%). Because of CIPs chains, the mechanical properties of matrix can be improved with increasing of the CIPs mass fractions. Moreover, the magnetic particles form the chain-like structures during the pre-structure process and the chains become denser with the particles' contents increase, thus the shear storage modulus (G) of the MRE increases. The initial modulus (G_0) of 2FF-MRE-unpre increases with the CIPs mass fraction (figure 4(c)). As shown in figure 4(d), the initial modulus of 2FF-MRE significantly increases due to the formation of CIPs chains in the pre-structure. Hence, the movability of the polymer matrix is reduced and the matrix is hardened.

Figure 4(e) illustrates the magnetic induced modulus of 2FF-MRE-unpre with different CIPs mass fractions. The magnetic induced modulus is defined as $\Delta G = G - G_0$. Since the shear storage modulus changing continuously under applying the magnetic field, the ΔG also changes, demonstrating the rheological properties of the material are enhanced. By applying the magnetic field, the magnetic energy of the material increases with the mass fraction of the CIPs. In this case, the distance among the CIPs particles decreases, so the magnetic induced modulus gradually increases. As shown in figure 4(f), the magnetic induced modulus of 2FF-MREs with different CIPs mass fractions is 0.1 MPa (30 wt%), 0.7 MPa (50 wt%), 2.6 MPa (70 wt%), respectively. During the pre-structure process, the CIPs are driven to assemble the chain-like structure. After the curing, the external magnetic field is turned off, and the CIPs are released to the balance under the interaction of elastic polymer and CIPs dipolar-dipolar force. The CIPs reach the lowest energy state without the magnetic field, thus the initial storage modulus is relatively low. Once the magnetic field is applied again, the CIPs chains become compact and the rheological properties are significantly improved (figure S1, supplementary information). With increasing of the CIPs mass fractions, the shear storage modulus of FF-MRE is obviously higher than the FF-MRE-unpre due to the unique chain structures.

3.3. Effect of flax fiber layers on MRE properties

The influence of flax fiber layers on the mechanical properties of FF-MRE properties is also explored. As shown in figure 5(a), the maximum shear storage modulus of FF-MRE-50 wt% increases from 1.1 MPa to 2.3 MPa with the incorporated flax fiber layer number rises from 0 to 4. Keeping the CIPs mass fraction at 50 wt% (figure 5(b)), the maximum shear storage modulus of isotropic pure MRE, 1FF-MRE-unpre, and 1FF-MRE is found to be 0.3 MPa, 0.6 MPa and 1.3 MPa, respectively. With the addition of flax fiber, the flax fiber is firmly embedded in the matrix and tightly bonded to the matrix. The shear storage modulus of the isotropic MRE is increased and the strength of the matrix is improved. In the pre-structure process, since the CIPs form chain-like structures, the flax fiber penperdicularly interacts with the CIPs chains to form the unique 3D topologic structures. The shear storage modulus of MRE is significantly increased, and the mechanical properties of the material are obviously improved. Figure 5(c) illustrates the corresponding magnetic induced modulus of MREs, of which the isotropic pure MRE-50 wt% is only 0.1 MPa and 2FF-MRE-50 wt% is 0.7 MPa. Compared to the isotropic MRE, after adding two layers of flax fiber to the matrix, the shear storage modulus of 2FF-MRE mainly depends on the enhancement of the matrix by the 3D topological structure and the binding interaction between the flax fibers and polymer matrix. The movement of the binding PDMS molecular chains is constrained, and the shear storage modulus obviously increases. The experimental results show that the magnetic induced modulus is increased significantly and the rheological properties of MRE are improved.

Figure 5(d) shows the magnetic hysteresis loop of FF-MRE-50 wt% with different flax fiber layers. The M_s of MRE and 1FF-MRE, 2FF-MRE, 3FF-MRE, 4FF-MRE is 106.0 emu g^{-1}, 101.1 emu g^{-1}, 100.3 emu g^{-1}, 97.6 emu g^{-1}, 97.2 emu g^{-1}, respectively. Because the relative content of CIPs decreases with increasing of the fiber layers under the same volume, the magnetization density decreases slightly. Interestingly, though the M_s value reduces, the mechanical properties of MREs are significantly enhanced by introducing the flax fiber into the PDMS matrix. Through the above structure analysis, it is found that the novel 3D topological structures are formed in the FF-MRE by perpendicularly interacted flax fiber and CIPs chains. With increasing of the flax fiber layers, a more compact 3D topological structure is achieved. In our work, too many flax fiber layers decrease the MR effect due to increment the initial modulus of FF-MRE (figures S2(a), (b)). Therefore, the 2 layers of flax fiber are selected as the optimum experimental conditions.

3.4. Effect of vulcanization conditions on MRE properties

The vulcanization conditions, such as vulcanization agent ratios and pre-structure time, also play important roles in determining the mechanical properties of MRE. The polymer matrix in the present MRE is PDMS, and the Sylgard 184 is used as the vulcanizing agent. Figures 6(a)–(c) illustrate the SEM images of 2FF-MRE-50 wt%, with different vulcanization ratios ranging from 10:1, 20:1 to 30:1, respectively. Before vulcanization, the PDMS macromolecule chains are linear, and they form spatial network structures after the vulcanization reaction. With increasing of the vulcanization ratios, the density of PDMS macromolecules becomes more

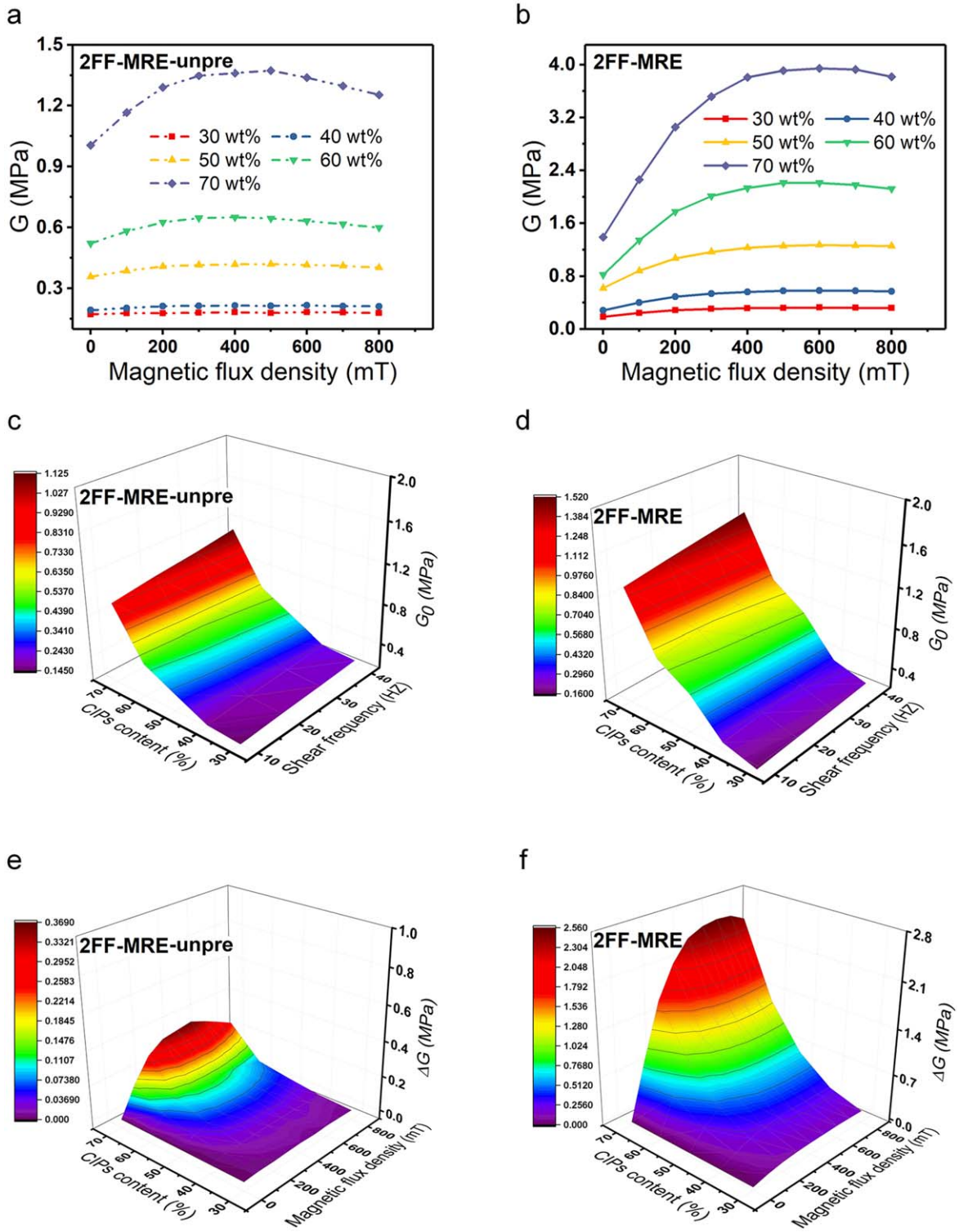

Figure 4. Under different CIPs mass fractions: Shear storage modulus of (a) 2FF-MRE-unpre and (b) 2FF-MRE; Initial storage modulus of (c) 2FF-MRE-unpre and (d) 2FF-MRE; Magnetic induced modulus of (e) 2FF-MRE-unpre and (f) 2FF-MRE.

concentrated. When the vulcanization ratio is reduced, the crosslinking nodes in the matrix are also reduced and the movement of the PDMS molecular chains is enhanced. Therefore, due to the weak binding force between the matrix molecular chains, the particles are easy to move in the matrix under the applied magnetic field. As a result, more compact CIPs chain-like structures are obtained.

Figure 6(d) illustrates the influence of crosslink ratios on the shear storage modulus of 2FF-MRE and 2FF-MRE-unpre when the CIPs mass fraction is 50 wt%. When the crosslink ratio is 30:1 and 20:1, the maximum shear storage modulus of 2FF-MRE-50 wt% reaches 1.0 MPa and 1.4 MPa, respectively. When an external magnetic field is applied, the particle motion in the matrix depends mainly on the amount of matrix

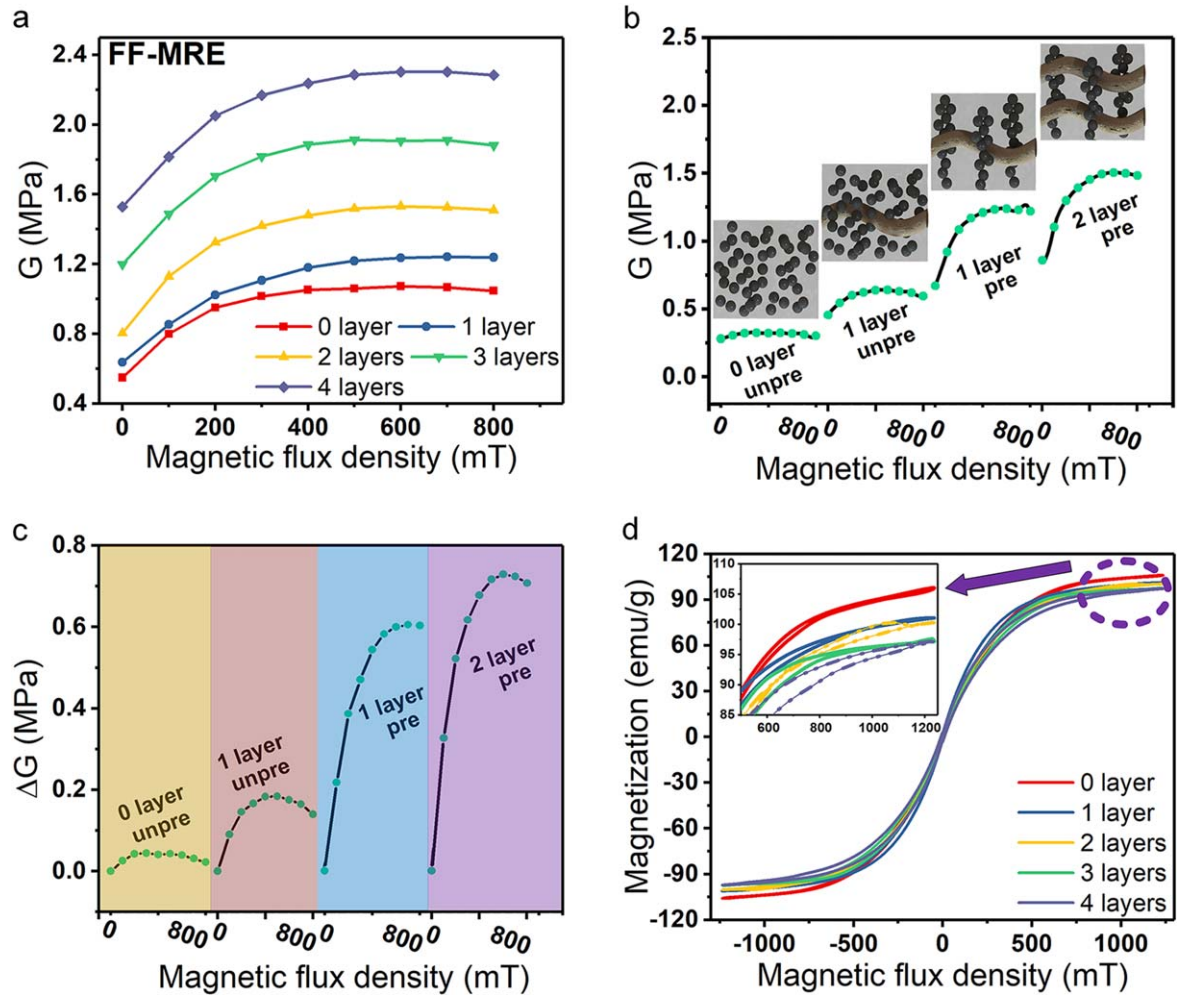

Figure 5. The influence of different layers of flax fiber: (a) shear storage modulus of FF-MRE-50 wt%, (b) shear storage modulus and (c) magnetic induced modulus of FF-MRE and FF-MRE-unpre with the CIPs mass fraction was 50 wt%; (d) Hysteresis loop of FF-MRE-50 wt% with different flax fiber layers.

binding force. When the crosslink ratio is high, the CIPs are tightly confined within the PDMS matrix, and they are difficult to move the position in the matrix. As we all know, the shear storage modulus is proportionally related to the crosslink density. The higher crosslink ratio leads to more crosslink nodes and larger binding forces are needed for CIPs to overcome to move in the matrix. Therefore, the shear storage modulus of MRE increases gradually by increasing the crosslink ratio.

Flax fiber and CIPs form the 3D topological structure in the FF-MRE and they surround parts of the PDMS matrix. When the FF-MRE is subjected to the external excitation, the external load needs to overcome the protection of the 3D topological structure to reach the surrounded PDMS. The PDMS which is located outside the 3D topological structure is defined as free rubber, while the PDMS located inside the 3D topological structure is defined as restrained rubber. The initial modulus of MRE is depended on not only the 3D topological structure, but also the effect of restrained rubber. Therefore, with increasing of the crosslink ratio, the number of restrained rubber gradually rises and the initial modulus increases significantly (figure 6(e)). Figure 6(f) shows the relative MR effect of 2FF-MRE-50 wt% and 2FF-MRE-unpre-50 wt%. When the crosslink ratio of the 2FF-MRE-50 wt% is 20:1, the MR effect reaches 91%. However, the MR effect is only 21% when the crosslink ratio is 10:1. This result indicates that the improvement of the vulcanization ratio leads to a gradual increase of the initial modulus, and decreases the MR effect.

Keeping the magnetic field (1 T) and temperature (100 °C) as constants, the shear storage modulus of FF-MREs prepared with 7 pre-structure time of 0, 3, 6, 9, 12, 15 and 30 min are investigated (figure 6(g)). Both the shear storage modulus and initial modulus increase steadily with increasing of the pre-structure time (figure 6(h)). For example, the initial modulus is 1.0 MPa (0 min), 1.8 MPa (3 min), 2.2 MPa (9 min), 2.3 MPa (15 min), and 2.6 MPa (30 min), respectively. When the crosslink ratio, CIPs mass fraction and flax fiber layers are fixed, the pre-structure time becomes the only factor affecting the CIPs motion and matrix structure. With increasing of the pre-structure time, the number of restrained rubber is increased and the chain-like structures become denser. As shown in figure 6(i), the MR effect of 2FF-MRE-70 wt% increases from 35% (0 min) to 127% (15 min).

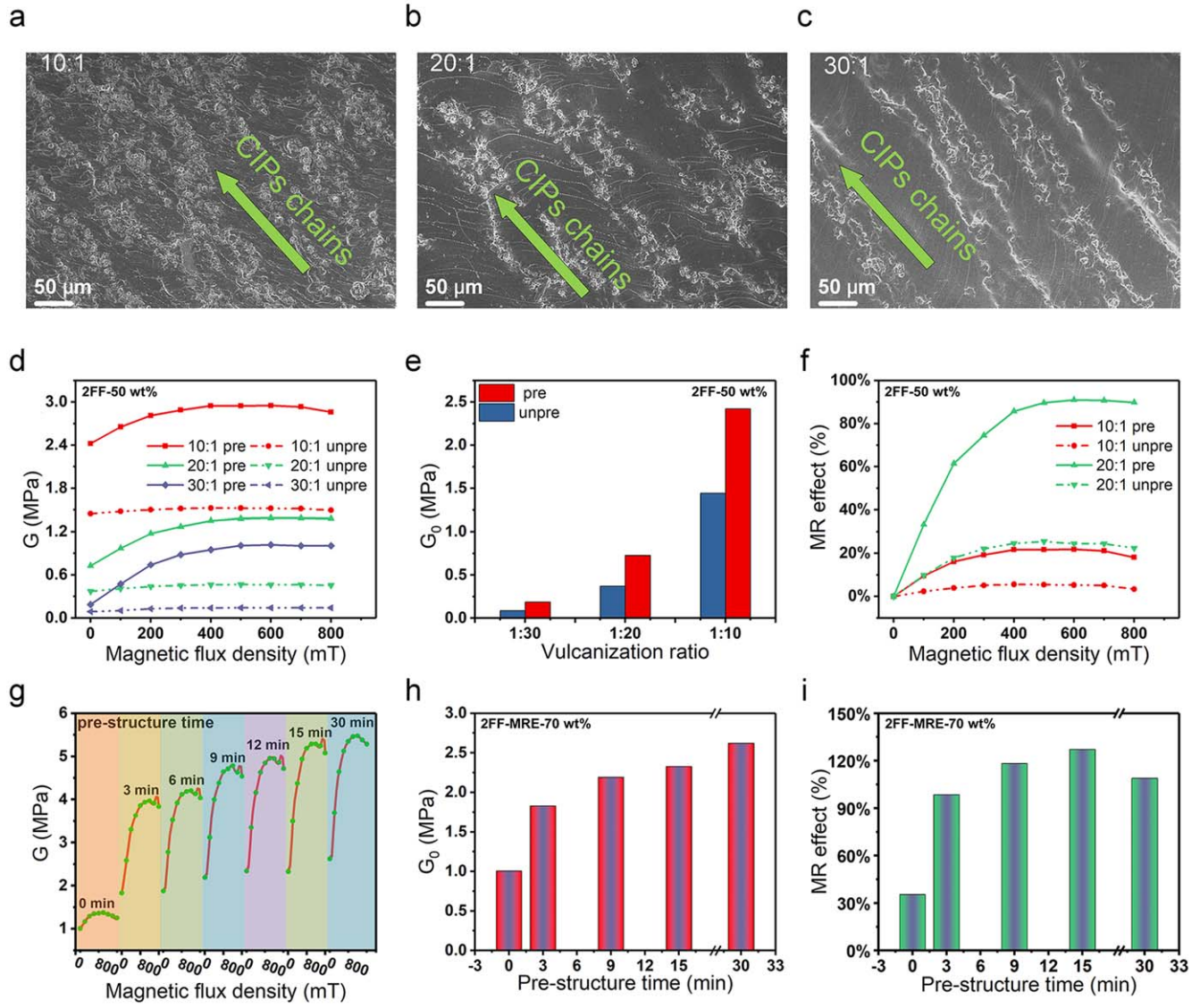

Figure 6. (a)–(c) SEM images of 2 FF-MRE-50 wt% with different vulcanization ratios; The CIPs mass fraction is 50 wt%: (d) Shear storage modulus, (e) initial modulus and (f) MR effect of 2FF-MRE and 2FF-MRE-unpre with different vulcanization ratios; (g) Shear storage modulus, (h) initial modulus and (i) MR effect of 2FF-MRE-70 wt% with different pre-structure time.

However, the MR effect decreases to 109% when the pre-structure time is 30 min. The cross-linking bonds are formed when the cross-linkable free radicals react with the rubber molecular chains. With increasing of the pre-structure time, the initially formed cross-linking bonds undergo shortening, rearrangement, cracking reactions, and the cross-link reactions finally tend to be completed. When the pre-structure time is 15 min, the matrix structure is stable and the cross-link reactions are completed, forming the CIPs chain-like structures. Therefore, the high MR effect is achieved because the 3D topological structure becomes stable. When the pre-structure time is longer than 15 min, there is a rearrangement of the crosslink, but the main reaction is the thermal pyrolysis reaction between the crosslinking bonds and the segments. As a result, the mechanical properties of the matrix decrease and this phenomenon is called over-curing. Therefore, when the pre-structure time is too long, the over-curing phenomenon results in the decreasing of mechanical properties.

The vulcanization conditions also affect the FF-MRE performance. With increasing of the vulcanization ratios, the mechanical properties of FF-MRE are enhanced significantly, but the rheological properties decrease gradually. The CIPs move freely in the matrix and completely form the chain-like structures with the pre-structure time increases, which significantly improve the mechanical properties of FF-MRE. When the pre-structure time is longer than 15 min and enters the over-curing stage, the rheological properties of FF-MRE decrease, so the pre-structure time of 15 min is selected as the experimental conditions.

In this study, the mechanical properties of FF-MRE are essentially improved by the 3D topological structure comprising of the CIPs chain-like structures and the flax fiber. Figures 7(a)–(d) show SEM images of the FF-MRE under applying the magnetic field with different times. Clearly, the particles are forced to assemble chain structures and the distribution of particle chains becomes much denser with

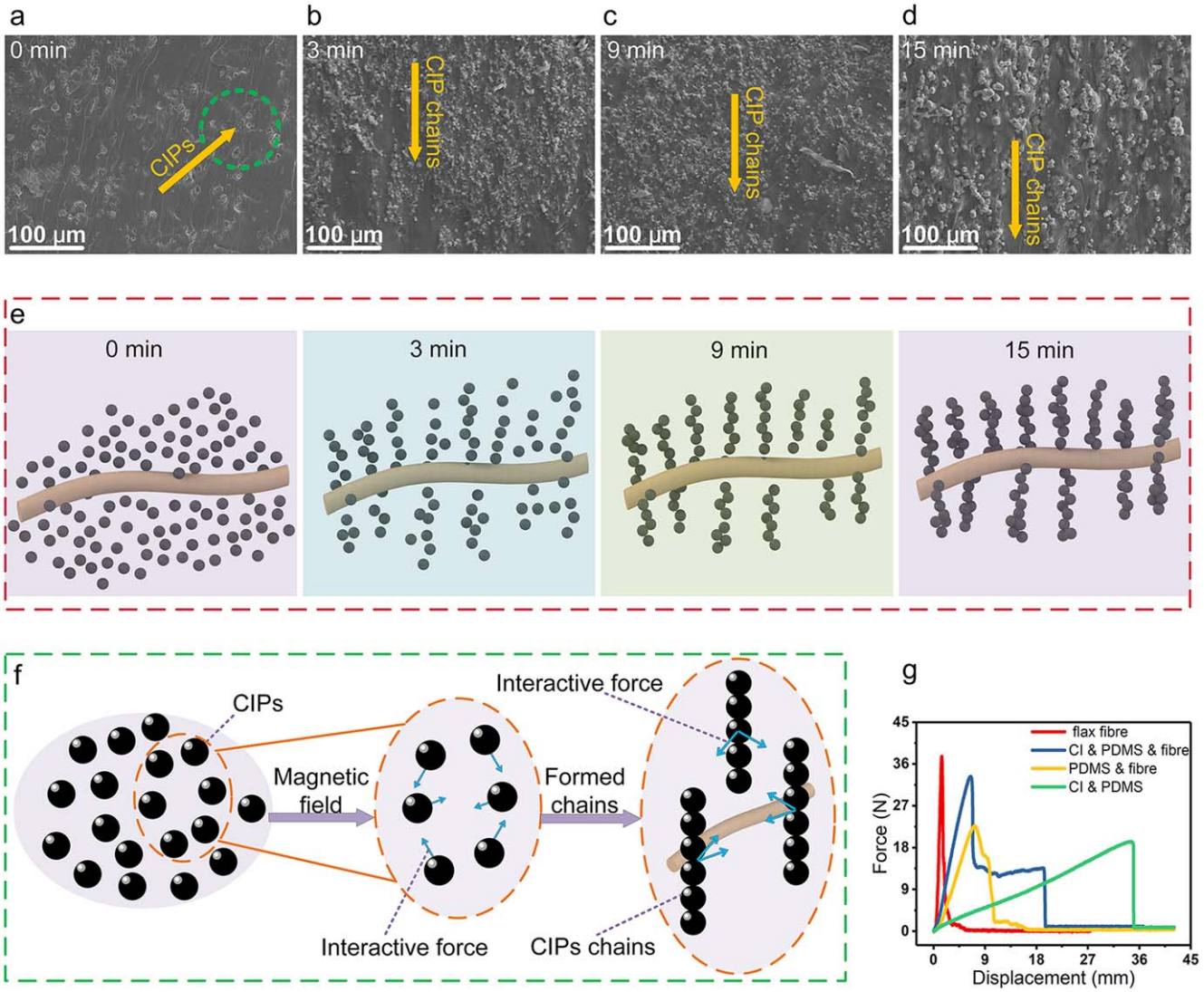

Figure 7. Schematic illustration of forming 3D topologic structure of 2FF-MRE-70 wt% under applying the magnetic field with different pre-structure time: (a)–(d) SEM images and (e) process of forming chains; (f) Mechanism diagram of the interaction among the CIPs-CIPs and chains-chains; (g) Comparison of tensile fracture of different materials.

increasing of the pre-structure time. In order to further describe the formation of particle chains, figure 7(e) shows the schematic of the time dependent chain-like structures formed by CIPs. When the pre-structure time was 0 min, particles were distributed randomly in the matrix. The CIPs gradually aggregated and showed chain-like structures (3 min). The CIPs gradually formed chain-like structures (9 min), which perpendicularly interacted with flax fiber to form stable 3D topological structures within the matrix. Meanwhile, the rubber entered in the flat stage of curing (positive cured time). During this stage, the cross-linking reaction tended to be completed, the reaction rate was alleviated, and the vulcanized rubber maintained the best performance. When the pre-structure time was 15 min, the CIPs were in the lowest energy state and the amount of restrained rubber reached the maximum value, which illustrated the FF-MRE was in the highest storage modulus state. With the pre-structure time continued to increase, FF-MRE entered in the over-curing stage. Figure 7(f) shows the CIPs motion under applying the magnetic field and the interaction of particles-particles and chains-chains. The CIPs were gradually magnetized, and the particles attracted with each other. Then, CIPs gradually formed chain-like structures with the pre-structure time increased. After the formation of CIPs chains, the interaction between the particle chains and the matrix kept the relative balance of the CIPs chains under the external magnetic field.

In order to investigate the effect of flax fiber on the tensile properties of MRE in detail, the tensile tests of pure flax fiber, pure MRE, PDMS package flax fiber and 1FF-MRE were conducted. As shown in figure 7(g), the fracture forces of a single flax fiber, 1 FF-MRE, PDMS packaged flax fiber, and pure MRE are 37.7 N, 33.3 N, 22.7 N, and 19.3 N, respectively. It is clear that the flax fiber plays the dominant role in improving the parallel direction performance of MRE. When the CIPs and flax fiber are simultaneously added into MRE, the tensile fracture strain of 1FF-MRE is much smaller than pure MRE, and the tensile fracture stress of 1FF-MRE is

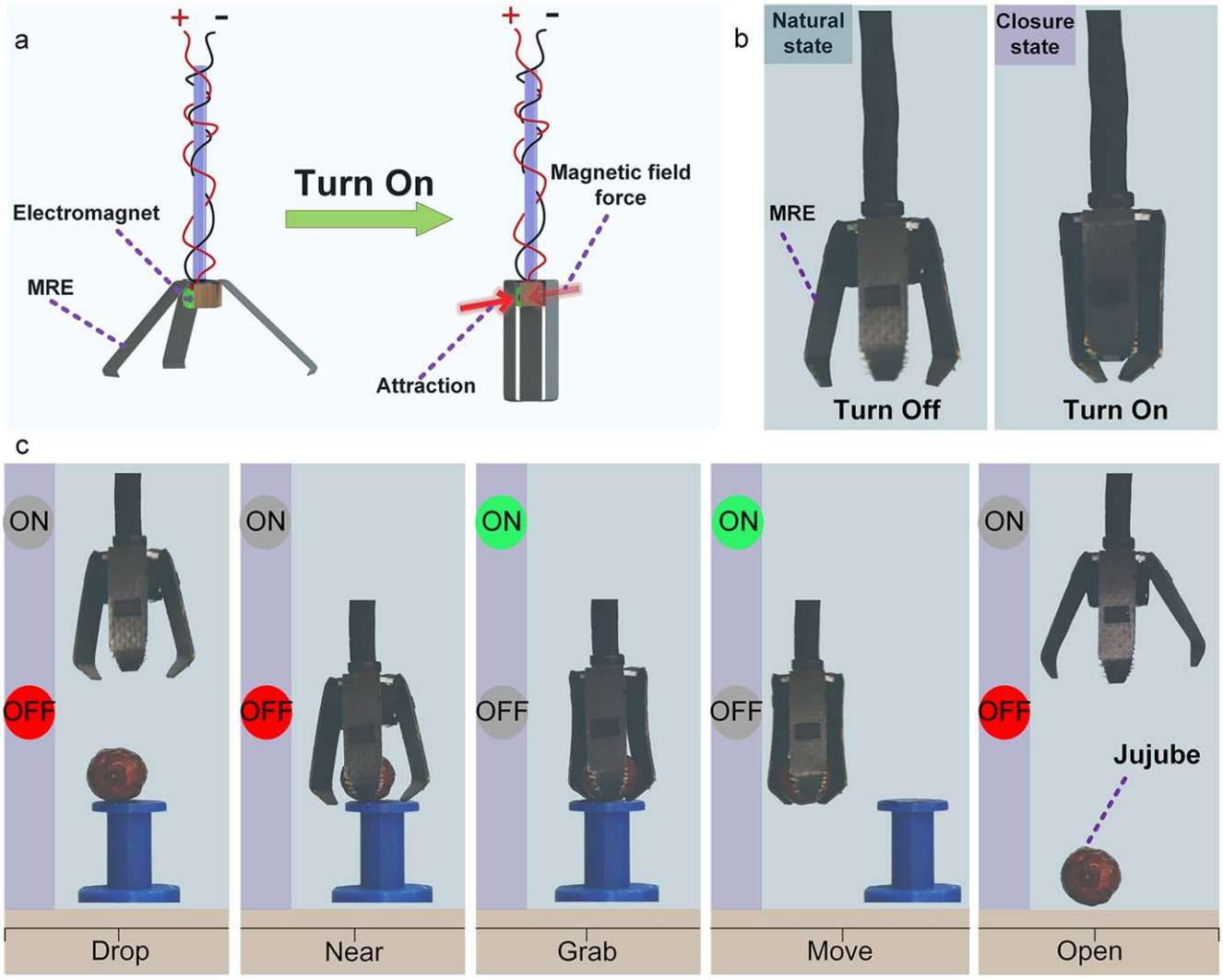

Figure 8. FF-MRE used as a gripper for transporting objects: (a) The diagram of gripper close and open; (b)The gripper open in the natural state and close after power turned on; (c) Schematic diagram of the grabbing jujube process.

larger than pure MRE. As a result, the Young's modulus of 1FF-MRE is much larger than pure MRE.

3.5. Designation of magnetic gripper based on the FF-MRE

Owing to the wonderful mechanical properties, the FF-MRE has broad potential in smart devices such as a magnetic gripper. Previously, the scholars fixed and energized the electromagnet which could generate a variable magnetic field, so that the gripper could be closed or opened by lifting the gripper towards or away from the electromagnet. Differently, this study installs small electromagnets at the root of the gripper. As shown in figure 8, the gripper is made up of FF-MRE with three pieces. The tip of each piece was bent to a certain angle according to the actual situation to form hook-like structures. The strength and bending angle of the gripper can be adjusted by controlling the fiber layers and CIPs content. The flaky samples are combined using a plastic rod to make a flexible gripper. By controlling the applied current to electromagnet, the real-time opening and closing function of the gripper is realized, and the goal of grasping and moving object is achieved. The gripper is open in the natural state, and the attraction of the magnetic field generated by energizing the electromagnet makes the gripper closed (figures 8(a), (b)). Because the magnetic field is generated by the root electromagnet of the flexible gripper, the gripper can be moved to elsewhere according to the actual requirements. Here, the illustrated gripper is only controlled by a on-off switch and more control system approach involved in the precise actuation is under studying. Figure 8(c) shows the process of grabbing-moving-releasing a jujube by using the FF-MRE gripper (movie S3). Firstly, the gripper is opened from the natural state to grab the jujube and moved freely until the power is turned off to loosen the object. The whole process is completed without hindrance. The gripper is composed of PDMS matrix, CIPs and flax fiber, which can resist the high temperature and the acid and alkali corrosion better. In addition, the gripper fabricated in this study is very convenient in practical application, which can be applied to some special conditions.

4. Conclusion

In summary, a novel FF-MRE with excellent mechanical-magnetic coupling characteristic is prepared by combining CIPs, flax fiber and PDMS matrix. When the CIPs mass fractions gradually increase, the initial modulus and magnetic induced modulus of FF-MRE have been greatly improved. The flax fiber and CIPs chains formed the 3D topologic structure within the FF-MRE matrix, which largely improves the matrix strength and mechanical properties of FF-MRE. Rheological properties and tensile strength of FF-MRE are obviously enhanced with increasing of the flax fiber layers. The vulcanization ratio affects the cross-link density of matrix, and further improves the strength of matrix. With the 3D topological structure, the number of restrained rubber gradually increases, which enhances the matrix strength and mechanical properties of FF-MREs. Under the condition of pre-structure, the vertical interaction of flax fiber and particle chains is more obviously, thus the matrix is strengthened. With increasing of the pre-structure time, the chain-like structures in the matrix become denser and the MR effect increases under the optimum condition. Due to the high mechanical property, the FF-MRE can be extended in active control and intelligent actuator, such as a flexible and controllable gripper.

Acknowledgments

Financial supports from the National Natural Science Foundation of China (Grant Nos. 11822209, 11572309) and Strategic Priority Research Program of the Chinese Academy of Sciences (Grant No. XDB22040502) are gratefully acknowledged. This work is also supported by the Collaborative Innovation Center of Suzhou Nano Science and Technology.

ORCID iDs

Xinglong Gong https://orcid.org/0000-0001-6997-9526

References

[1] Bastola A K and Li L 2018 A new type of vibration isolator based on magnetorheological elastomer *Mater. Design.* **157** 431–6
[2] Li Y C, Li J C, Tian T F and Li W H 2013 A highly adjustable magnetorheological elastomer base isolator for applications of real-time adaptive control *Smart Mater. Struct.* **22** 095020
[3] Sun S S, Chen Y, Yang J, Tian T F, Deng H X, Li W H, Du H and Alici G 2014 The development of an adaptive tuned magnetorheological elastomer absorber working in squeeze mode *Smart Mater. Struct.* **23** 075009
[4] Sun S S, Deng H X, Yang J, Li W H, Du H, Alici G and Nakano M 2015 An adaptive tuned vibration absorber based on multilayered MR elastomers *Smart Mater. Struct.* **24** 045045
[5] Yang Z R, Qin C Y, Rao Z S, Ta N and Gong X L 2014 Design and analyses of axial semi-active dynamic vibration absorbers based on magnetorheological elastomers *J. Inter. Matsyst. Str.* **25** 2199–207
[6] Zhang X Z and Li W H 2009 Adaptive tuned dynamic vibration absorbers working with MR elastomers *Smart Struct. Syst.* **5** 517–29
[7] Caterino N, Azmoodeh B M and Occhiuzzi A 2014 Medium to long term behavior of MR dampers for structural control *Smart Mater. Struct.* **23** 117005
[8] Maddaloni G, Caterino N and Occhiuzzi A 2017 Shake table investigation of a structure isolated by recycled rubber devices and magnetorheological dampers *Struct. Control Hlth.* **24** e1906
[9] Mikhailov V P, Bazinenkov A M, Dolinin P A and Stepanov G V 2018 Research on the dynamic characteristics of a controlled magnetorheological elastometer damper *Instrum. Exp. Tech.* **61** 427–32
[10] Bica I 2011 Magnetoresistor sensor with magnetorheological elastomers *J. Ind. Eng. Chem.* **17** 83–9
[11] Tian T F, Li W H and Deng Y M 2011 Sensing capabilities of graphite based MR elastomers *Smart Mater. Struct.* **20** 025022
[12] Akhavan H, Ghadiri M and Zajkani A 2019 A new model for the cantilever MEMS actuator in magnetorheological elastomer cored sandwich form considering the fringing field and Casimir effects *Mech. Syst. Signal. Pr.* **121** 551–61
[13] Ding L, Xuan S H, Feng J B and Gong X L 2017 Magnetic/conductive composite fiber: a multifunctional strain sensor with magnetically driven property *Compos. Part A-Appl.* S **100** 97–105
[14] Gao W, Wang L, Wang X and Liu H 2016 Magnetic driving flowerlike soft platform: biomimetic fabrication and external regulation *ACS Appl. Mater. Inter.* **8** 14182–9
[15] Liu Q, Li H and Lam K Y 2018 Transition of magnetic field due to geometry of magneto-active elastomer microactuator with nonlinear deformation *J. Microelectromech.* S **27** 127–36
[16] Zhou G Y and Wang Q 2005 Design of a smart piezoelectric actuator based on a magnetorheological elastomer *Smart Mater. Struct.* **14** 504
[17] Feng J B, Xuan S H, Ding L and Gong X L 2017 Magnetoactive elastomer/PVDF composite film based magnetically controllable actuator with real-time deformation feedback property *Compos. Part A-Appl.* S **103** 25–34
[18] Nguyen V Q, Ahmed A S and Ramanujan R V 2012 Morphing soft magnetic composites *Adv. Mater.* **24** 4041–54
[19] Li W H and Nakano M 2013 Fabrication and characterization of PDMS based magnetorheological elastomers *Smart Mater. Struct.* **22** 055035
[20] Sorokin V V, Ecker E, Stepanov G V, Shamonin M, Monkman G J, Kramarenko E Y and Khokhlov A R 2014 Experimental study of the magnetic field enhanced Payne effect in magnetorheological elastomers *Soft Matter* **10** 8765–76
[21] Kaleta J, Królewicz M and Lewandowski D 2011 Magnetomechanical properties of anisotropic and isotropic magnetorheological composites with thermoplastic elastomer matrices *Smart Mater. Struct.* **20** 085006
[22] Sapouna K, Xiong Y P and Shenoi R A 2017 Dynamic mechanical properties of isotropic/anisotropic silicon magnetorheological elastomer composites *Smart Mater. Struct.* **26** 115010
[23] Yu M, Ju B, Fu J, Liu X and Yang Q 2012 Influence of composition of carbonyl iron particles on dynamic mechanical properties of magnetorheological elastomers *J. Magn. Magn. Mater.* **324** 2147–52

[24] An J S, Kwon S H, Choi H J, Jung J H and Kim Y G 2017 Modified silane-coated carbonyl iron/natural rubber composite elastomer and its magnetorheological performance *Compos. Struct.* **160** 1020–6
[25] Khimi S R and Pickering K L 2016 The effect of silane coupling agent on the dynamic mechanical properties of iron sand/natural rubber magnetorheological elastomers *Compos. Part B-Eng.* **90** 115–25
[26] Vasudevan M P, Sudeep P M, Al-Omari I A, Kurian P, Ajayan P M, Narayanan T N and Anantharaman M R 2015 Enhanced microactuation with magnetic field curing of magnetorheological elastomers based on iron–natural rubber nanocomposites *B. Mater. Sci.* **38** 689–94
[27] Li R and Sun L Z 2013 Viscoelastic responses of silicone-rubber-based magnetorheological elastomers under compressive and shear loadings *J. Eng. Mater. Technol.* **135** 021008
[28] von Lockette P R, Lofland S E, Koo J-H, Kadlowec J and Dermond M 2008 Dynamic characterization of bimodal particle mixtures in silicone rubber magnetorheological materials *Polym. Test.* **27** 931–5
[29] Qi S, Yu M, Fu J, Li P D and Zhu M 2015 Creep and recovery behaviors of magnetorheological elastomer based on polyurethane/epoxy resin IPNs matrix *Smart Mater. Struct.* **25** 015020
[30] Yu M, Qi S, Fu J, Zhu M and Chen D 2017 Understanding the reinforcing behaviors of polyaniline-modified carbonyl iron particles in magnetorheological elastomer based on polyurethane/epoxy resin IPNs matrix *Compos. Sci. Technol.* **139** 36–46
[31] Ge L, Gong X L, Wang Y and Xuan S H 2016 The conductive three dimensional topological structure enhanced magnetorheological elastomer towards a strain sensor *Compos. Sci. Technol.* **135** 92–9
[32] An H, Picken S J and Mendes E 2012 Nonlinear rheological study of magneto responsive soft gels *Polymer* **53** 4164–70
[33] Ju B, Yu M, Fu J, Zheng X and Liu S 2013 Magnetic field-dependent normal force of magnetorheological gel *Ind. Eng. Chem. Res.* **52** 11583–9
[34] Rao P V, Maniprakash S M, Srinivasan S M and Srinivasa A R 2010 Functional behavior of isotropic magnetorheological gels *Smart Mater. Struct.* **19** 085019
[35] Yang C, Wu L and Li G 2018 Magnetically responsive superhydrophobic surface: *in situ* reversible switching of water droplet wettability and adhesion for droplet manipulation *ACS Appl. Mater. Inter.* **10** 20150–8
[36] Hu Y, Wang Y L, Gong X Q, Gong X L, Zhang X Z, Jiang W Q, Zhang P Q and Chen Z Y 2005 New magnetorheological elastomers based on polyurethane/Si-rubber hybrid *Polym. Test.* **24** 324–9
[37] Lai N T, Ismail H, Abdullah M K and Shuib R K 2019 Optimization of pre-structure parameters in fabrication of magnetorheological elastomer *Arch. Civ. Mech. Eng.* **19** 557–68
[38] Shi G Q, Wang W J, Lu H L, Wang G P, Yang F F and Rui X T 2019 Study of crosslink structure and dynamic mechanical properties of magnetorheological elastomer: effect of vulcanization system *J. Intel. Mat. Syst. Str.* **30** 1189–99
[39] Huang W J, Dai K, Zhai Y, Liu H, Zhan P F, Gao J C, Zheng G Q, Liu C T and Shen C Y 2017 Flexible and lightweight pressure sensor based on carbon nanotube/thermoplastic polyurethane-aligned conductive foam with superior compressibility and stability *ACS Appl. Mater. Inter.* **9** 42266–77
[40] Qin Y Y *et al* 2015 Lightweight, superelastic, and mechanically flexible graphene/polyimide nanocomposite foam for strain sensor application *ACS Nano* **9** 8933–41
[41] Rinaldi A, Tamburrano A, Fortunato M and Sarto M 2016 A flexible and highly sensitive pressure sensor based on a PDMS foam coated with graphene nanoplatelets *Sensors* **16** 2148
[42] Yin X, Vinod T P and Jelinek R 2015 A flexible high-sensitivity piezoresistive sensor comprising a Au nanoribbon-coated polymer sponge *J. Mater. Chem.* C **3** 9247–52
[43] Ge L, Xuan S H, Liao G J, Yin T T and Gong X L 2015 Stretchable polyurethane sponge reinforced magnetorheological material with enhanced mechanical properties *Smart Mater. Struct.* **24** 037001
[44] Gong X L, Wang Y, Hu T and Xuan S H 2017 Mechanical property and conductivity of a flax fiber weave strengthened magnetorheological elastomer *Smart Mater. Struct.* **26** 075013
[45] Liu Q and Hughes M 2008 The fracture behaviour and toughness of woven flax fiber reinforced epoxy composites *Compos. Part A-Appl.* S **39** 1644–52